Non-covalent bridging of bithiophenes through chalcogen bonding grips

Deborah Romito,[a] Nicolas Biot,[a] Francesco Babudri,[b] and Davide Bonifazi*,[a]

In this work, chalcogen-functionalized dithiophenes, equipped on both extremities with chalcogen-bonding recognition heterocycles, have been prepared following two synthetic pathways. The insertion of the chalcogenazolo[5,4-β]pyridine allows the control of the organization at the solid state. X-Ray diffraction analysis of the single crystals, showed that the Te-doped derivatives give the most persistant assemblies, with the molecules arranging at solid-state in wire-like polymeric structures through Te···N interactions. As expected, the introduction of the Se and Te atoms, dramatically decreases the emission properties, with the Te-bearing congeners being virtually non emissive.

Introduction

During the last decades, academic research experienced a strong surge of interest in the field of molecular[1] and polymeric[2] organic semiconducting materials to engineer flexible and printed electronics.[3] The advantage of using organic materials rather than inorganic counterparts resides in the fact that one can tailor the molecular HOMO-LUMO gap by organic functionalization of the pi-conjugated scaffold. Changing the length[4] and the nature[5] of the carbon-based framework, as well as altering its composition by replacing selected carbon atoms with isostructural analogues (known as heteroatom-doping),[6] embody some of the main approaches used to tailor the photophysical properties of molecular materials. Moreover, depending on the structural modification, different molecular arrangements can be obtained in the solid state, and materials with poor organisation could give devices with reduced performances.[7] Therefore, growing attention has been given to the use of non-covalent interactions to master molecular arrangements at the solid state.

Along with the fine tuning of the photophysical properties,[8] the use of heavy chalcogen atoms (Se and Te) in small molecules could allow the control of the molecular organization through chalcogen-bonding interactions (EBIs).[9] The chalcogen bond belongs to the family of Secondary Bonding Interactions (SBIs).[10] A SBI include electrostatic (described as σ-hole), orbital mixing and van der Waals contributions. The orbital contribution is typically described as $n^2(Y)\rightarrow\sigma^*(E\text{-}X)$ donation (X-E···Y), where non-bonding electrons of the electron-donating atom Y interact with the empty antibonding σ^*_{X-E} orbital located on E atom (with E being a central polarizable atom and X its substituent). EBIs have found significant application in crystal engineering,[11] where macrocyclic[12] and wire-like[13] assemblies could be easily form. Our group provided its contribution to the field when we prepared Te- and Se-bearing molecular modules able to form supramolecular polymers at the solid state through single Y···E interactions.[14] Aiming at improving the persistency of the recognition, we have developed the chalcogenazolo[5,4-β]pyridine (CGP) scaffold,[15] providing an important contribution to the family of supramolecular synthons acting as both chalcogen bond donors and acceptors.[16] This ambivalent nature allows to observe non-covalent dimerization at the solid state, through the formation of double EBIs arranged into a six-membered ring.[17] In view of integrating the EBI as tool for controlling the solid-state organization of conducting oligothiophenes in organic electronics,[18] in this work we describe our initial efforts to master the self-assembly of the shortest units, namely the dithiophene. In particular, we report on the functionalisation of dithienyl modules that, terminating with chalcogenazole moieties, establish EBIs at the solid state, forming controlled assemblies (Scheme 1). In analogy with results previously described,[14, 18h] one would anticipate that the S and N atoms of the thiophene and azole rings engage in intramolecular EBIs, forcing the chalcogenazolo and thiophenyl units to adopt a locked flat conformation.[18h] It is also expected that the presence of a heavy chalcogen atom should dramatically influence the photophysical properties of the dithienyl derivatives. At the retro-synthetic planning level, we considered the insertion of

[a] Deborah Romito, Dr. Nicolas Biot, Prof. Dr. Davide Bonifazi School of Chemistry, Cardiff University
Main Building, Park Place
Cardiff CF10 3AT (United Kingdom)
E-mail:bonifazid@cardiff.ac.uk

[b] Prof. Dr. Francesco Babudri
Dipartimento di Chimica
Università degli Studi Aldo Moro di Bari
Via Orabona 4
70126 Bari (Italy)

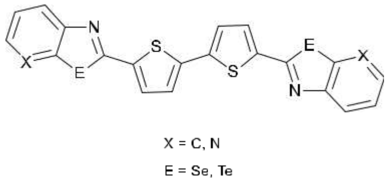

Scheme 1. Chemical structures of chalcogen-functionalized bithiophenes.

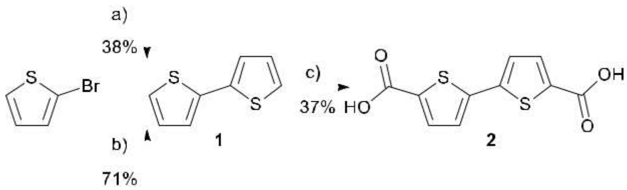

Scheme 2. Synthetic pathway for the bithiophene-based core **2**. Reagents and condition: a) thiophen-2-ylboronic acid, 6 mol% $Pd(PPh_3)_4$, Na_2CO_3, toluene, EtOH, 90 °C, overnight; b) thiophen-2-ylmagnesium bromide, 1 mol% $NiCl_2$(dppp) , Et_2O, reflux, 3 h; c) 1. *n*-BuLi, Et_2O, -78 °C to r.t., 2 h; 2. CO_2, -78 °C for 2 h, r.t. overnight.

the chalcogen-containing moiety in two steps, the dehydrative cyclization reaction to chalcogenazoles, and the amide disconnection.

Results and discussion

Synthetic procedures

The synthesis started with the preparation of 2,2'-bithiophene **1**. While the Suzuki-Miyaura coupling reaction between 2-bromothiophene with thiophen-2-ylboronic acid led to **1** in 40% of yield, Kumada cross-coupling of thiophen-2-ylmagnesium bromide with 2-bromothiophene in the presence of $NiCl_2$(dppp) gave the desired product in 71% of yield. Molecule **1** was then capped with carboxylic acid groups by treating the corresponding solution in Et_2O with *n*-BuLi at -78 °C, followed by the addition of gaseous CO_2 (Scheme 2). Following synthetic routes from the literature,[19] we prepared dichalcogenide $\mathbf{4_{Se}}$ and $\mathbf{4_{Te}}$ from 2-bromoaniline **3**. In parallel, pyridyl analogues $\mathbf{6_{Se}}$ and $\mathbf{6_{Te}}$ were prepared in low yields starting from 3-amino-2-bromopyridine (Scheme 3).[15] The syntheses of derivatives $\mathbf{7_{X\text{-}E}}$ were accomplished by reductive cleavage of the dichalcogenide bond in the presence of $NaBH_4$, followed by the alkylation of the chalcogenide intermediate with MeI in good to excellent yields (Scheme 3). Dicarboxamide derivatives $\mathbf{8_{X\text{-}E}}$ were obtained through amide bond formation upon reaction with $\mathbf{2_{Cl}}$, which was obtained from $\mathbf{2_{OH}}$ after treatment with $SOCl_2$.

Dehydrative cyclization to give bis-selenazoles and -tellurazoles $\mathbf{9_{X\text{-}E}}$ was performed using $POCl_3$ and NEt_3 as a base, according to the synthetic protocol developed in our group (Scheme 3a-f).[14] It has to be noted that difficulties in purifying bisamide $\mathbf{8_{C\text{-}Te}}$ led us to perform the final step with the crude material. Precisely, the intermediate monocarboxamides were identified in all crude mixtures from the amidation reactions, suggesting that the poor solubility of the intermediates could prevent the full conversion into final products $\mathbf{9_{X\text{-}E}}$. Consequently, we attempted

a different synthetic path, using Te-containing amines $\mathbf{7_{X\text{-}Te}}$ reacting with the acyl chloride of the commercially available 5-

bromothiophene-2-carboxylic acid, freshly generated after treatment with $SOCl_2$. Amides $\mathbf{10_{X\text{-}Te}}$ were converted into the corresponding cyclized derivatives $\mathbf{11_{X\text{-}Te}}$**,** following the same protocol used for $\mathbf{8_{X\text{-}E}}$. Finally, a one-pot borylation/Suzuki-

Miyaura coupling (BSC) was performed, converting brominated compounds $\mathbf{11_{X\text{-}Te}}$ *in situ* into the boronate derivatives, by treatment with B_2Pin_2 and KOAc in the presence of the Pd catalyst. Although we proved the chemical compatibility of the

tellurazole derivatives with the Pd-catalysed reaction conditions, the overall yields for products $\mathbf{9_{X\text{-}Te}}$ did not overcome those reached for the direct bis-functionalization of **2**. All unknown molecules were characterized by ^{1}H-NMR spectroscopy, IR, m.p. and HR-mass spectroscopy (see Supporting Information). Unfortunately, ^{13}C-NMR spectra could not be reported for the entire set of compounds because of poor solubility, likely due to their tendency to aggregate in solution through EBIs.

Solid-state arrangement

The strong tendency for aggregation, limited the growth of crystals suitable for X-Ray diffraction analysis. Despite the numerous attempts, amorphous powders were obtained for both pyridyl-based molecules $\mathbf{9_{N\text{-}Se}}$ and $\mathbf{9_{N\text{-}Te}}$. We obtained X-ray crystal structures for benzochalcogenazoles $\mathbf{9_{C\text{-}Se}}$ and $\mathbf{9_{C\text{-}Te}}$. In addition, the solid-state arrangement of monofunctionalized thiophenes $\mathbf{11_{X\text{-}Te}}$ was also unravelled from crystals obtained by slow evaporation of a $CHCl_3$ solution. Figures 1 and 2 display the ORTEP representation and the crystal packing for each molecule.

Crystals of the solvate of $\mathbf{9_{C\text{-}Se}}$ were obtained by slow evaporation (Figures 1a-1d). As predicted (see above), the Se atoms adopt a *syn*-type conformation due to the formation of intramolecular S···N EBIs. Interestingly, in this crystal packing it is the solvent molecules that, bridging neighbouring molecular unit of $\mathbf{9_{C\text{-}Se}}$ through concurring hydrogen and chalcogen bonds (Figure 1b), drive the solid-state arrangement. A weak Se···Cl SBI is observed ($d_{Se\cdots Cl}$ = 3.617 Å < sum of vdW radii = 3.65 Å, C_7-Se_1···Cl_1 = 154.4°), whereas nitrogen and sulphur atoms act as hydrogen-bonding acceptors with the acidic hydrogen atoms of $CHCl_3$ molecules ($d_{N\cdots C}$ = 3.388 Å; $d_{S\cdots C}$ = 3.646 Å). The interactions with the solvent generate a ribbon-like supramolecular architecture (Figure 1c). Additional π-π stacking interactions govern the formation of the columnar arrangements, in which each S atom of the monomers through a S···S interaction ($d_{S\cdots S}$ = 3.584 Å) and a S···C interaction ($d_{S\cdots C}$ = 3.466 Å) respectively (Figure 1d).

C-Te

As far as molecule **9** is concerned, very small crystals were obtained by slow cooling from a hot *p*-xylene solution (Figures 1e-i). Unlike crystals for **9C-Se**, the solvent is not included in the solid, and the molecular arrangement is likely to be predominately driven by Te···N SBIs (*d*Te···N = 3.431 Å < sum of vdW radii = 3.61 Å, C7-Te1···N1 = 156.9°, Figure 1f). Each chalcogen-bonding grip engages with neighbouring molecules

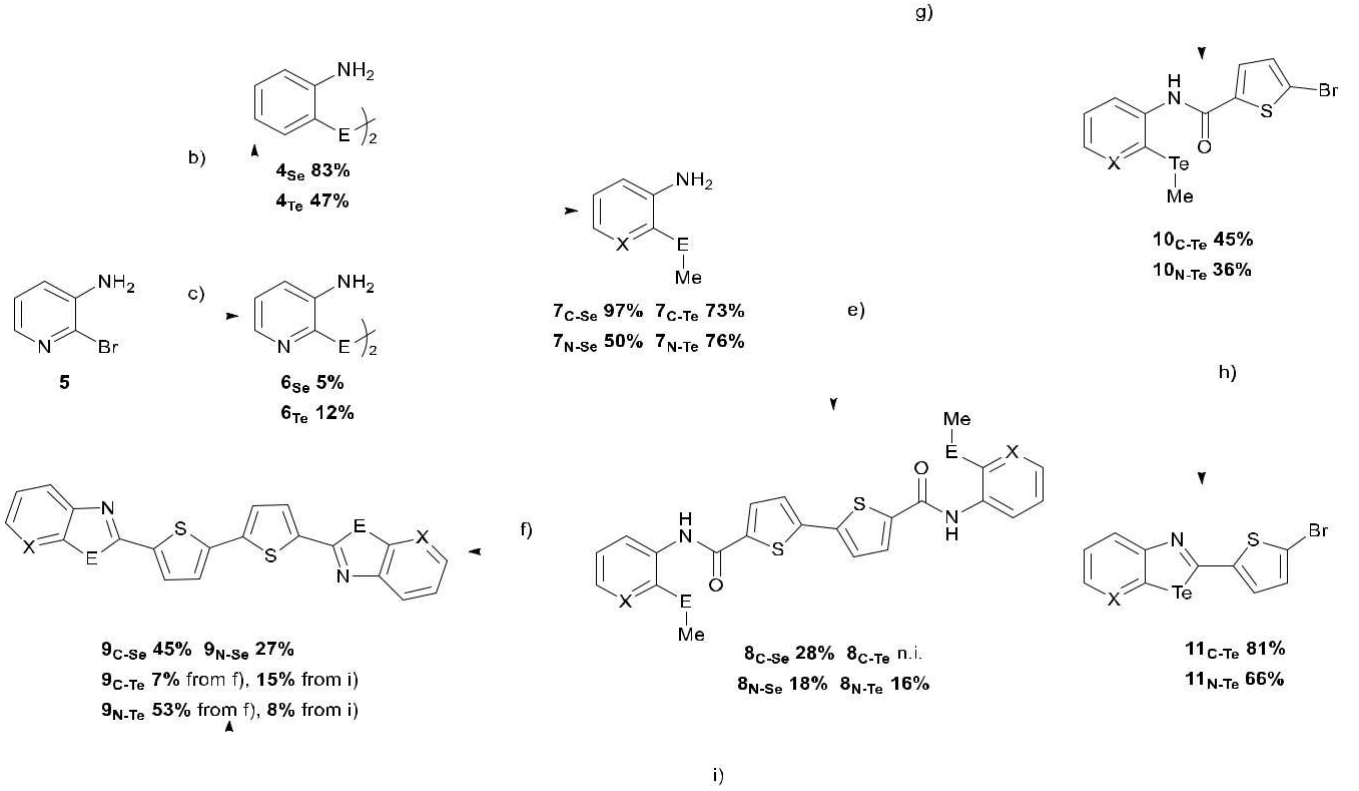

Scheme 3. Synthetic pathway to **9**. Reagents and conditions: a) 1. *t*-BuLi, THF, -78 °C to r.t., 3 h; 2. Se^0, r.t., overnight; 3. $K_3Fe(CN)_6$, H_2O, r.t., 10'; b) 1. NaH, Te^0, NMP, 185 °C, 3.5 h; 2. NH_4Cl, H_2O, air, r.t., 2 h; c) 1. *i*-PrMgCl, THF, 0 °C to r.t., 3 h; 2. E^0, r.t., overnight; 3. Se: $K_3Fe(CN)_6$, H_2O, r.t., 10', Te: NH_4Cl, H_2O, air, r.t., 2 h; d) 1. $NaBH_4$, MeOH, THF, r.t., 1.5 h; 2. CH_3I, r.t., 1.5 h; e) 1. **2** in $SOCl_2$, reflux, overnight; 2. NEt_3, 5 mol% DMAP, $CHCl_3$, reflux, 24 h; n.i. = not isolated; f) $POCl_3$, NEt_3, 1,4-dioxane, reflux, overnight; g) 1, $SOCl_2$, reflux, overnight; 2. NEt_3 for $\mathbf{7_{C\text{-}Te}}$, pyridine for $\mathbf{7_{N\text{-}Te}}$, CH_2Cl_2, 0 °C to r.t., overnight; h) $POCl_3$, NEt_3, 1,4-dioxane, reflux, overnight; i) 3 mol% $Pd_2(dba)_3$, 1 mol% XPhos, B_2Pin_2, KOAc, 1,4-dioxane, 110 °C, 27 h.

with a different role in the EBI. Namely, one takes part in an EBI as a chalcogen bonding donor (having the Te atom implicated), whereas the other acts as EBI acceptor through the N atom (Figure 1g). This peculiar recognition pattern forces the molecules to adopt a non-planar arrangement, and a braided double wire-like architecture is formed (Figure 1i).

Moving to the crystals of monomeric derivatives $\mathbf{11_{X\text{-}Te}}$, one can notice the presence of shorter chalcogen bonds, likely due to the presence of the electron-withdrawing Br atom. The Br atom also actively takes part to the development of the supramolecular assembly through the formation of halogen-bonding interactions. Both crystals grew by slow evaporation of

a $CHCl_3$ solution, but the data quality of $\mathbf{11_{C\text{-}Te}}$ is poorer than that obtained with tellurazolopyridine analogue $\mathbf{11_{N\text{-}Te}}$; the structure is, indeed, disordered, thus the major component of the disorder has been used for the following discussion (for the

actual crystal structure, see SI).

In the case of $11_{C\text{-}Te}$ (Figures 2a-c), two monomers form the asymmetric unit of the crystal structure, each of them interacting with a neighbouring molecule through two SBIs. One side of each molecule sees both the σ-holes of the Te atoms involved as SBI donors, whereas the opposite side takes up the

nitrogen and sulfur atoms as SBI acceptors (Figure 2b - for monomer 1: $d_{Te\cdots N}$ = 3.284 Å < sum of vdW radii = 3.61 Å, $C_7\text{-}Te_1\cdots N_1$ = 158.9° and $d_{Te\cdots S}$ = 3.774 Å < sum of vdW radii = 3.86 Å, $C_1\text{-}Te_1\cdots S_1$ = 168.7°; for monomer 2: $d_{Te\cdots N}$ = 3.285 Å < sum of vdW radii = 3.61 Å, $C_{18}\text{-}Te_{2A}\cdots N_{2A}$ = 158.2° and $d_{Te\cdots S}$ = 3.763 Å < sum of vdW radii = 3.86 Å, $C_{12A}\text{-}Te_{2A}\cdots S_{2A}$ = 170.4°). As observed for molecule $9_{C\text{-}Te}$, the molecular arrangement does not follow a coplanar organization (Figure 2c). Halogen-halogen

interaction bridges two neighbouring molecules along the *a* axis of the cell ($d_{Br\cdots Br}$ = 3.624 Å < sum of vdW radii = 3.7 Å, $C_{22A}\text{-}Br_{2A}\cdot\cdot Br_1$ = 173.2°), whereas weak chalcogen-chalcogen

contacts drives the stacking of the molecules along the *b* axis ($d_{Te\cdots Te}$ = 4.076 Å). The crystal structure of $11_{N\text{-}Te}$ confirms the expected recognition fidelity of the tellurazolopyridine, depicting the presence of the double chalcogen-bonded array

(Figures 2d-f); indeed, the interactions between Te and N atoms of neighbouring pyridyl rings are observed (Figure 2e - $d_{Te\cdots N}$ = 2.981 Å < sum of vdW radii = 3.61 Å; $C_6\text{-}Te_1\cdots N_2$ = 165.6 °C). Furthermore, a third molecule (not involved in the formation of dimeric complexes) bridges two couples of dimers through a

S···H hydrogen bond, with the thienyl S atom acting as a hydrogen-bonding acceptor ($d_{S\cdots C}$ = 3.578 Å). Differently from benzotellurazole analogue $11_{C\text{-}Te}$, in the crystals of $11_{N\text{-}Te}$ the bromine atom participates in the development of the

supramolecular architecture through Br···C interactions ($d_{Br\cdots C}$ = 3.484 Å) with the pyridyl ring (i.e., through π-σ*orbital

interactions). Notably, the crystal packing develops following a herringbone arrangement, with the molecules arranging in a wave-type fashion along the *b* axis of the cell. In the "wavy" arrangement, the molecules are held together through π-π stacking interactions, engaging both the carbon atoms of the thienyl ($d_{C\cdots C}$ = 3.398 Å) and pyridyl ($d_{C\cdots C}$ = 3.375 Å) rings (Figure 2f).

Formation of macroscopic morphologies

The formation of macroscopic morphologies for **9$_{C\text{-}Te}$** was also investigated by Atomic Force Microscopy (AFM) after drop-cast deposition on mica surfaces. Homogeneous coverage of the surface with **9$_{C\text{-}Te}$** was observed, but a zoomed picture reveals the presence of several elongated and layered "islands", likely due to a disordered aggregation of amorphous material (Figure 3b). The same surface was then examined after solvent vapour annealing (SVA): as shown in Figure 3c, the morphology outcome is drastically changed, with the entire surface covered by needle-like aggregates (Figures 3d-3e). The distribution of the nanostructures is reminiscent of the braided arrangement observed in the crystal structure, having the needle-like objects disposed according to a zig-zag pattern on the surface.

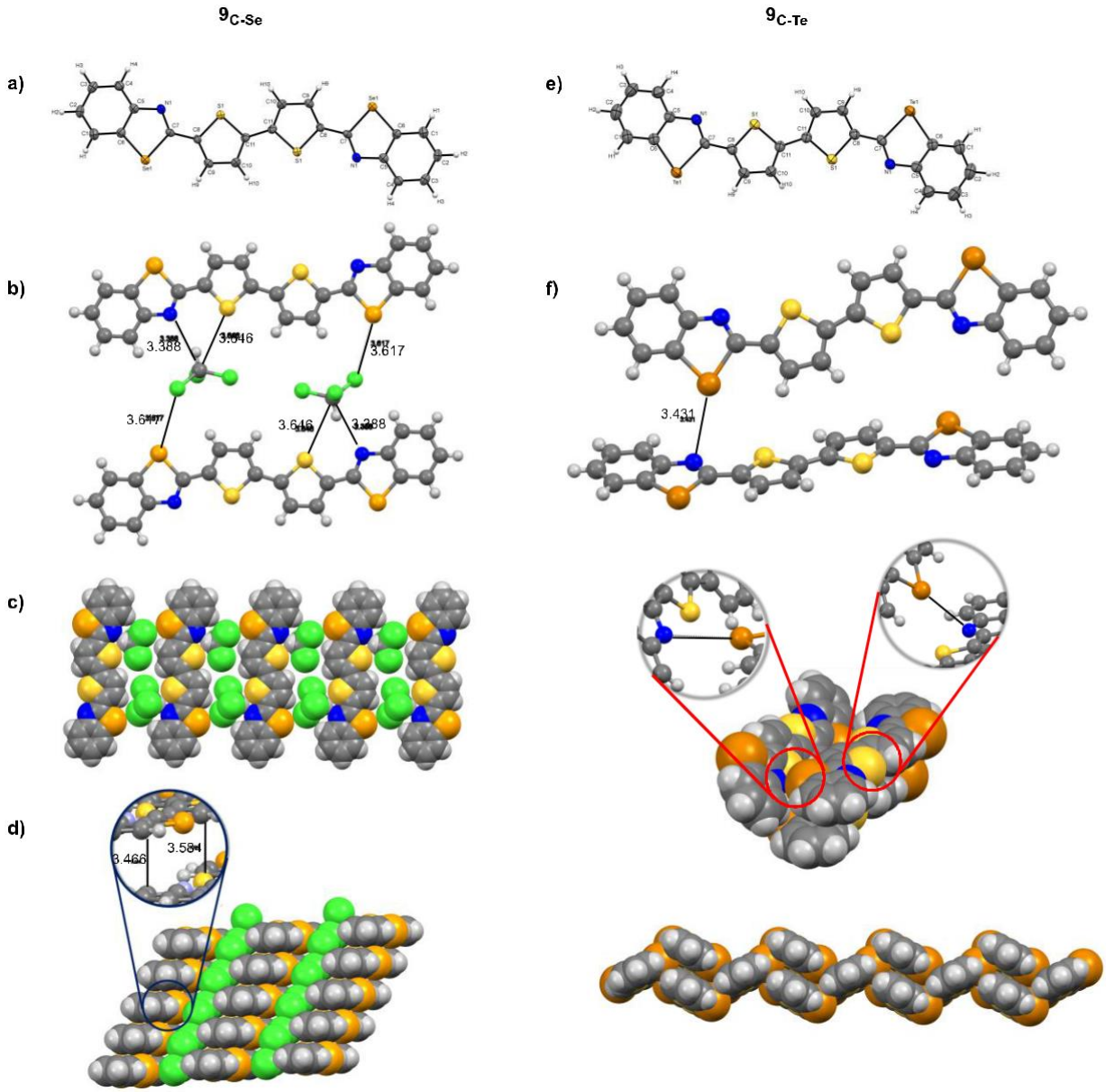

Fig. 1. On the left a) ORTEP representation of a single molecule of **9$_{C\text{-}Se}$**; b) evidence of SBIs and H-bonds, distances are expressed in Å; c) van der Waals (vdW) radii representation of the crystal packing according to a ribbon organization; d) vdW representation of the crystal packing with a zoom to highlight the intermolecular π-π distances (expressed in Å). Solvent of crystallization: $CHCl_3$. Space group: P-1. On the right e) ORTEP representation of a single molecule of **9$_{C\text{-}Te}$**; f) crystal unit of **9$_{C\text{-}Te}$** with chalcogen bond highlighted, distances are expressed in Å; g) vdW representation of the crystal packing with a zoom to highlight the different chalcogen bonds involving both the sides of the same molecule; i) vdW radii representation of the crystal packing according to a braided double wire-like organization. Solvent of crystallization: *p*-xylene. Space group: P $2_1/c$

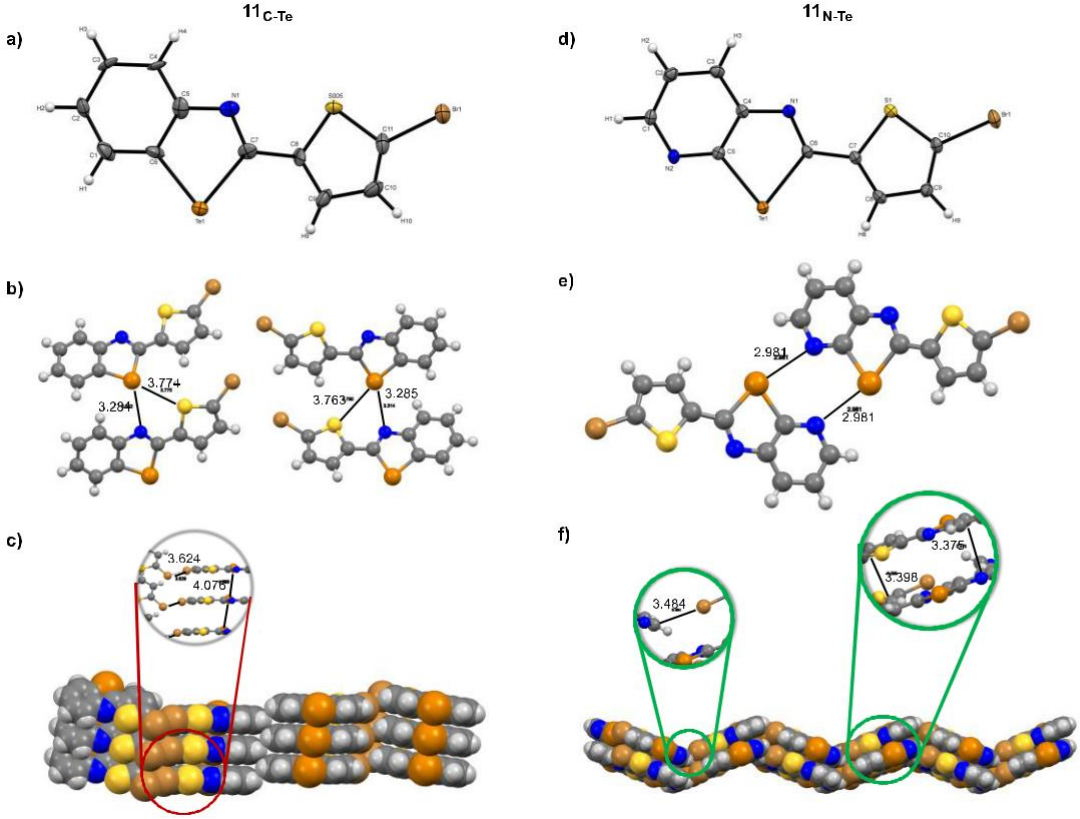

Fig. 2. On the left a) ORTEP representation of a single molecule of **11$_{C-Te}$**; b) crystal unit of **11$_{C-Te}$** with chalcogen bonds highlighted, distances are expressed in Å; c) vdW representation of the crystal packing with an enlargement to highlight the additional halogen-halogen and chalcogen-chalcogen interactions (distances are expressed in Å). Solvent of crystallization: $CHCl_3$. Space group: $Pna2_1$. On the right d) ORTEP representation of a single molecule of **11$_{N-Te}$**; e) crystal structure of **11$_{N-Te}$** showing the formation of dimeric complexes with chalcogen bonds highlighted, distances are expressed in Å; f) vdW representation of the crystal packing according to a double wave-like organization, with an enlargement to highlight the halogen bond and the π-π distances (expressed in Å). Solvent of crystallization: $CHCl_3$. Space group: Pbcn.

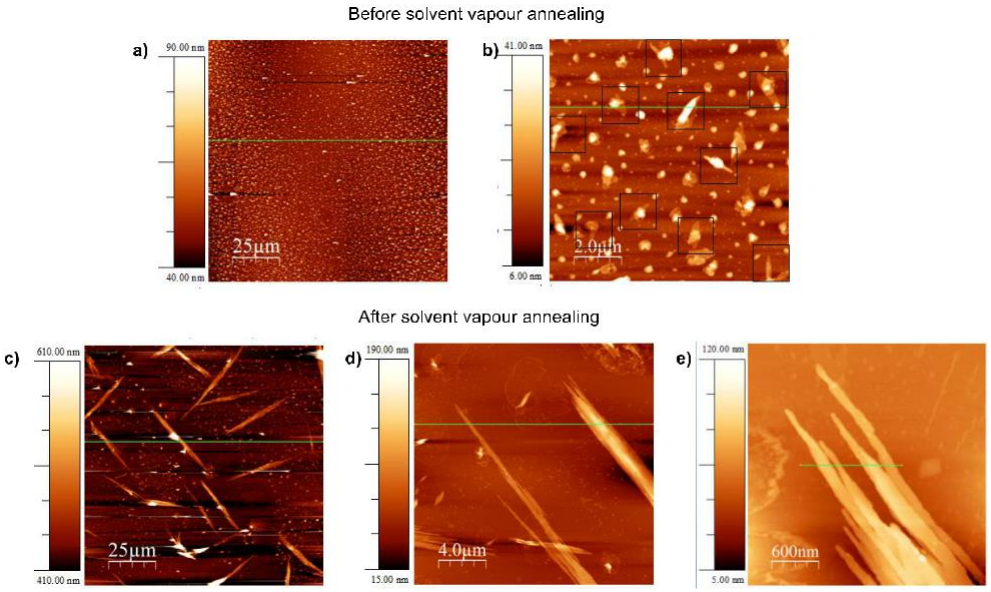

Fig. 3. Top: AFM images of the surface prepared by drop coating of a solution of **9$_{C-Te}$** in $CHCl_3$, a) AFM image of the whole surface (125 x 125 µm); b) AFM zoomed image of the surface (10 x 10 µm), showing layered islands (highlighted by black squares). Bottom: AFM images of the surface after solvent vapour annealing treatment, c) AFM image of the whole surface (125 x 125 µm); d) AFM zoomed image showing in detail one of the needle-like objects (20 x 20 µm); e) Additional AFM zoomed image showing one of the extremities of the needle-like objects (3 x 3 µm).

Absorption and emission spectroscopy

The effect of the Se and Te atoms on the photophysical properties of the dithiophene framework was evaluated by UV/Vis absorption and emission spectroscopy, and the key photophysical data are summarized in Table 1. In general, all compounds show low molar absorption coefficients.[19] Analysing bischalcogenazoles **9C-Se** and **9C-Te** and bischalcogenazolopyridine derivatives **9N-Se** and **9N-Te** separately, batochromic shifts were noticed when passing from the Se- to the Te-bearing congeners.

A broadening of the vibrational structure becomes more evident as the mass of the chalcogen atom increases, as proven by the poorly structured band observed for **9N-Te** (Figure 4).[19] In terms of emission, weak emissive properties (fluorescence quantum yields: 0.03-0.08) were noticed in solution only for the Se-containing compounds at rt. Considering the presence of the heavy-atom Te atom, we conjectured that derivatives **9C-Te** and **9N-Te** (induced by the presence of the heaviest Te atom) could possess strong phosphorescent emission.[20] Unfortunately, steady state measurements demonstrated a pronounced fluorescence quenching descending from Se to Te. In parallel, no phosphorescence was detected for any of the derivatives at rt, nor in a 77 K glassy matrix.[19]

Experimental part

Bithiophene-based core **2**, dichalcogenides **4** and **6**, and methylchalcogenides **7** were prepared according to conditions reported in the literature (see SI). Commercial 2-bromothiophene, 5-bromothiophene-2-carboxylic acid, 2-bromoaniline and 3-amino-2-bromopyridine were used without additional purification. All the solvents were dried prior to use.

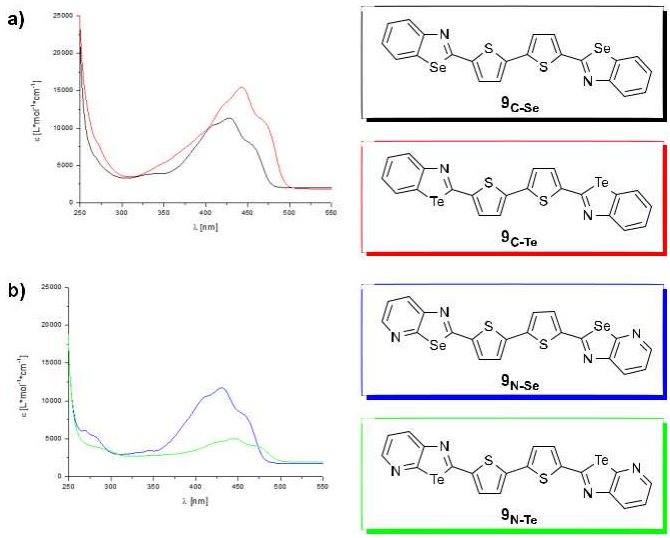

Fig. 4. a) Absorption spectra of the bisbenzochalcogenazoles **9C-Se** and **9C-Te** at 298 °K; b) absorption spectra of bischalcogenazolopyridines **9N-Se** and **9N-Te** at 298 °K. Solvent: $CHCl_3$.

Table 1. Optical properties for chalcogen-containing bithiophenes in $CHCl_3$ solutions.

Compound	λ [nm],[a] ε [M^{-1} cm^{-1}]	λ_{em} [nm],[b]	Φ_{fl}
9C-Se	428, 11580	416	0.08
9C-Te	443, 13900	n.d.	
9N-Se	432, 10100	421	0.03
9N-Te	445, 3300	n.d.	

[a] UV/Vis absorption maximum in $CHCl_3$ at 298 °K.

[b] Emission maximum in $CHCl_3$ at 298 °K; n.d. = not detected.

Preparation of dicarboxamides 8

A two-necked flask was loaded with 102 mg (0.4 mmol) of **2** under N_2. The solid was dissolved in 2.4 mL of $SOCl_2$, then the system was stirred at reflux overnight. Once the solvent was removed under vacuum, the resulting acyl chloride derivative was dissolved in 1 mL of $CHCl_3$ and DMAP (0.02 mmol) was added. This was followed by the addition of a solution of 0.18 mL of NEt_3 (1.28 mmol) and 0.88 mmol of the relevant substrate **7X-E** in 1.4 mL of $CHCl_3$. The reaction was stirred at reflux for 24 hours, water added, and the solution extracted with $CHCl_3$. The combined organic extracts were washed with brine, dried over Na_2SO_4, filtered and the solvents removed under reduced pressure. The crude materials were purified by silica gel chromatography.

Preparation of bisbenzochalcogenazole-containing bithiophenes 9C-Se and 9C-Te

To a suspension of corresponding dicarboxamides **8C-Se** or **8C-Te** (0.04 mmol) in 3.8 mL of 1,4-dioxane under N_2, 66 µL of NEt_3 (0.48 mmol) and a solution of $POCl_3$ (0.16 mmol) in 0.2 mL of 1,4-dioxane were added. The reaction was stirred at reflux overnight, diluted with $CHCl_3$ and washed with a saturated solution of $NaHCO_3$. The aqueous phase was extracted with $CHCl_3$, and the combined organic extracts washed with brine, dried over $MgSO_4$, filtered and the solvents removed under reduced pressure. The crude materials were purified by silica gel chromatography.

Preparation of CGP-containing bithiophenes 9N-Se and 9N-Te

To a suspension of corresponding dicarboxamides **8N-Se** or **8N-Te** (0.04 mmol) in 3.8 mL of 1,4-dioxane under N_2, 0.13 mL of NEt_3 (0.96 mmol) and a solution of $POCl_3$ (0.32 mmol) in 0.2 mL of 1,4-dioxane were added. The reaction was stirred at reflux overnight, diluted with $CHCl_3$ and washed with a saturated solution of $NaHCO_3$. The aqueous phase was extracted with $CHCl_3$, the combined organic extracts washed with brine, dried over Na_2SO_4, filtered and the solvents removed under reduced pressure. The crude materials were purified by silica gel chromatography.

Conclusions

In this paper, we have described the synthesis of two families of bithiophene-based materials, in which Se and Te atoms were inserted, and the chalcogen-containing functionalization was varied from benzo-1,3-chalcogenazoles to chalcogenazolo[5,4-β]pyridines. All compounds were characterized and the molecular organization at the solid state probed for bisbenzochalcogenazoles **9$_{C\text{-}Se}$** and **9$_{C\text{-}Te}$** and monofunctionalized thiophenes **11$_{C\text{-}Te}$** and **11$_{N\text{-}Te}$**. Furthermore, the macroscopic organisation of **9$_{C\text{-}Te}$** was studied on mica surfaces by AFM imaging techniques. The morphologies obtained by SVA and observed by AFM were revealed to be consistent with the molecular organisation determined by X-ray analysis, thus strengthening the idea that chalcogen bonds can be considered strong enough to develop a stable supramolecular structure both in crystals and on surfaces. These initial results could open the road toward the preparation of semiconducting materials displaying increasing complexity, with the oligothiophenyl cores functionalized with solubilizing alkyl chains and terminating with CGP grips. In our engineering approach, this would allow the formation of solids with controlled molecular organizations, expressing intermolecular EBIs, that would lead to materials with enhanced charge mobilities and optoelectronic property at large.

Conflicts of interest

There are no conflicts to declare.

Acknowledgements

D.B. gratefully acknowledges Cardiff University and the EU through the MSCA-RISE funding scheme (project INFUSION) for the financial support. The authors also acknowledge the use of the Advanced Computing (ARCCA) at Cardiff University, and associated support services. D.R. thanks the Global Thesis Fellowship program sponsored by the University of Bari Aldo Moro for supporting her master work at Cardiff University.

Notes and references

1. (a) M. Gershenson, V. Podzorov and A. Morpurgo, *Rev. Mod. Phys.*, 2006, **78**, 973-988; (b) Y. Chen, X. Wan and G. Long, *Acc. Chem. Res.*, 2013, **46**, 2645-2655.
2. (a) G. Yu, J. Gao, J. C. Hummelen, F. Wudl and A. J. Heeger, *Science*, 1995, **270**, 1789-1791; (b) A. Facchetti, *Chem. Mater.*, 2010, **23**, 733-758.
3. (a) H. Sirringhaus, T. Kawase, R. Friend, T. Shimoda, M. Inbasekaran, W. Wu and E. Woo, *Science*, 2000, **290**, 2123-2126; (b) A. M. Bagher, *Sustainable Energy*, 2014, **2**, 85-90.
4. H. Van Mullekom, J. Vekemans, E. Havinga and E. Meijer, *Mater. Sci. Eng. R*, 2001, **32**, 1-40.
5. C. Kitamura, S. Tanaka and Y. Yamashita, *Chem. Mater.*, 1996, **8**, 570-578.
6. U. N. Maiti, W. J. Lee, J. M. Lee, Y. Oh, J. Y. Kim, J. E. Kim, J. Shim, T. H. Han and S. O. Kim, *Adv. Mater.*, 2014, **26**, 40-67.
7. M. Olguin, R. R. Zope and T. Baruah, *J. Chem. Phys.*, 2013, **138**, 074306.
8. (a) E. I. Carrera and D. S. Seferos, *Macromolecules*, 2015, **48**, 297-308; (b) M. Al-Hashimi, Y. Han, J. Smith, H. S. Bazzi, S. Y. A. Alqaradawi, S. E. Watkins, T. D. Anthopoulos and M. Heeney, *Chem. Sci.*, 2016, **7**, 1093-1099.
9. (a) N. A. Pushkarevsky, A. V. Lonchakov, N. A. Semenov, E. Lork, L. I. Buravov, L. S. Konstantinova, G. T. Silber, N. Robertson, N. P. Gritsan and O. A. Rakitin, *Synth. Met.*, 2012, **162**, 2267-2276; (b) K. T. Mahmudov, M. N. Kopylovich, M. F. C. G. da Silva and A. J. Pombeiro, *Dalton Trans.*, 2017, **46**, 10121-10138; (c) N. Biot and D. Bonifazi, *Coord. Chem. Rev.*, 2020, **413**, 213243.
10. N. W. Alcock, in *Advances in Inorganic Chemistry and Radiochemistry*, Elsevier, 1972, vol. 15, pp. 1-58.
11. (a) A. F. Cozzolino, P. J. W. Elder and I. Vargas-Baca, *Coord. Chem. Rev.*, 2011, **255**, 1426-1438; (b) P. C. Ho, J. Rafique, J. Lee, L. M. Lee, H. A. Jenkins, J. F. Britten, A. L. Braga and I. Vargas-Baca, *Dalton Trans.*, 2017, **46**, 6570-6579; (c) P. Scilabra, G. Terraneo and G. Resnati, *Acc. Chem. Res.*, 2019, **52**, 1313-1324.
12. P. C. Ho, P. Szydlowski, J. Sinclair, P. J. Elder, J. Kübel, C. Gendy, L. M. Lee, H. Jenkins, J. F. Britten, D. R. Morim and I. Vargas-Baca, *Nat. Commun.*, 2016, **7**, 11299.
13. (a) D. B. Werz, R. Gleiter and F. Rominger, *J. Am. Chem. Soc.*, 2002, **124**, 10638-10639; (b) D. B. Werz, F. R. Fischer, S. C. Kornmayer, F. Rominger and R. Gleiter, *J. Org. Chem.*, 2008, **73**, 8021-8029.
14. A. Kremer, A. Fermi, N. Biot, J. Wouters and D. Bonifazi, *Chem. Eur. J.*, 2016, **22**, 5665-5675.
15. N. Biot and D. Bonifazi, *Chem. Eur. J.*, 2018, **24**, 5439-5443.
16. (a) M. Fourmigué and A. Dhaka, *Coord. Chem. Rev.*, 2020, **403**, 213084; (b) V. Kumar, Y. Xu, C. Leroy and D. L. Bryce, *PCCP*, 2020, **22**, 3817-3824.
17. Y. Lu, W. Li, W. Yang, Z. Zhu, Z. Xu and H. Liu, *Phys. Chem. Chem. Phys.*, 2019, **21**, 21568-21576.
18. (a) J. Roncali, *Chem. Rev.*, 1992, **92**, 711-738; (b) Y. Yamashita, K. Ono, S. Tanaka, K. Imaeda and H. Inokuchi, *Adv. Mater.*, 1994, **6**, 295-298; (c) M. Karikomi, C. Kitamura, S. Tanaka and Y. Yamashita, *J. Am. Chem. Soc.*, 1995, **117**, 6791-6792; (d) H. Brisset, S. Le Moustarder, P. Blanchard, B. Illien, A. Riou, J. Orduna, J. Garin and J. Roncali, *J. Mater. Chem.*, 1997, **7**, 2027-2032; (e) P. Frère, M. Allain, E. H. Elandaloussi, E. Levillain, F. X. Sauvage, A. Riou and J. Roncali, *Chem. Eur. J.*, 2002, **8**, 784-792; (f) F. Di Maria, P. Olivelli, M. Gazzano, A. Zanelli, M. Biasiucci, G. Gigli, D. Gentili, P. D'Angelo, M. Cavallini and G. Barbarella, *J. Am. Chem. Soc.*, 2011, **133**, 8654-8661; (g) G. C. Welch, R. C. Bakus, S. J. Teat and G. C. Bazan, *J. Am. Chem. Soc.*, 2013, **135**, 2298-2305; (h) H. Huang, L. Yang, A. Facchetti and T. J. Marks, *Chem. Rev.*, 2017, **117**, 10291-10318; (i) F. Di Maria, M. Zangoli, M. Gazzano, E. Fabiano, D. Gentili, A. Zanelli, A. Fermi, G. Bergamini, D. Bonifazi and A. Perinot, *Adv. Funct. Mater.*, 2018, **28**, 1801946; (j) R. Peng, H. Guo, J. Xiao, G. Wang, S. Tan, B. Zhao, X. Guo and Y. Li, *ACS Appl. Energy Mater.*, 2018, **1**, 2192-2199.

19. A. Kremer, C. Aurisicchio, F. De Leo, B. Ventura, J. Wouters, N. Armaroli, A. Barbieri and D. Bonifazi, *Chem. Eur. J.*, 2015, **21**, 15377-15387.

20. (a) G. He, W. Torres Delgado, D. J. Schatz, C. Merten, A. Mohammadpour, L. Mayr, M. J. Ferguson, R. McDonald, A. Brown, K. Shankar and E. Rivard, *Angew. Chem. Int. Ed.*, 2014, **53**, 4587-4591; (b) G. He, B. D. Wiltshire, P. Choi, A. Savin, S. Sun, A. Mohammadpour, M. J. Ferguson, R. McDonald, S. Farsinezhad, A. Brown, K. Shankar and E. Rivard, *Chem. Commun.*, 2015, **51**, 5444-5447; (c) S. M. Parke, M. P. Boone and E. Rivard, *Chem. Commun.*, 2016, **52**, 9485-9505; (d) M. Baroncini, G. Bergamini and P. Ceroni, *Chem. Commun.*, 2017, **53**, 2081-2093.